Constant Speed Parametrization Mapping of Curved Boundary Surfaces in Higher-Order Moment-Method Electromagnetic Modeling

Milan M. Ilić, *Member, IEEE*, Slobodan V. Savić, Andjelija Ž. Ilić, *Member, IEEE*, and Branislav M. Notaroš, *Senior Member, IEEE*

***Abstract*—A constant speed parametrization (CSP) mapping of boundary surfaces is proposed for moment-method analysis of antennas and scatterers, along with its approximation using large higher-order Lagrange-type curved quadrilateral patches. The importance of the proper placement of interpolation nodes that ensures minimum mapped parametric space distortion (arc-length parametrization) is explained and demonstrated on simple examples. The CSP mapping results in on average five times lower radar cross section (RCS) error for a spherical scatterer than with the ray casting (central projection) parametrization mapping. The extension of the CSP concept to arbitrary surfaces is illustrated in modeling of the double-ogive target.**

***Index Terms*—Curved parametric elements, electromagnetic analysis, geometrical mapping, higher-order modeling, moment methods, scattering.**

I. Introduction

RELATIVELY recently, the computational electromagnetics (CEM) community has started to extensively investigate and employ curvilinear elements for geometrical modeling of antennas and scatterers [1]–[9] because they offer greater modeling flexibility and enable larger elements to be used in meshes of arbitrary structures, particularly when combined with higher-order basis functions for currents and fields. Most frequently used curved parametric elements for CEM modeling by far are those involving polynomial parametrization (e.g., Lagrange interpolating polynomials, Bézier curves, and splines) [1]–[7], but more complex parametrization based on rational polynomial functions (e.g., rational Bézier curves and nonuniform rational B-splines or NURBS) has also been adopted in a number of works [8], [9]. Rational polynomial parametrization allows exact modeling of all conical sections (e.g., a circle) and can ensure constant surface tangents across element interconnects, but it comes at the cost of more complex implementation and impairing the overall polynomial structure, and thus the resulting opportunities for efficient nonredundant calculations of field integrals and generalized impedances (inner products) [3], when polynomial basis functions in parametric coordinates are used.

However, practically all works in curvilinear CEM modeling focus on definitions and implementations of particular basis functions on curved elements, as well as on evaluations of associated generalized impedances, i.e., integrals in the curvilinear space, and it appears that none of them address the problem of how to actually position the interpolation (control) nodes that guide the geometry of curved elements. On the other hand, the mapping from the element parent domain to its curvilinear form, typically done by some kind of projection, can be performed in an infinite number of ways. This problem, which apparently has not been adequately investigated and documented by CEM researchers, turns out to be especially important when higher-order large curvilinear elements are constructed and applied (e.g., Lagrange elements of orders higher than two, when more than three interpolation nodes per edge drive the element geometry).

This letter focuses on Lagrange-type generalized parametric quadrilaterals as basic geometrical boundary elements in the method of moments (MoM) analysis of metallic and dielectric antennas and scatterers within the surface integral equation (SIE) approach [3] and points out the importance of proper placement of interpolation nodes such that the resulting mapping introduces the least amount of parametric coordinate distortion in the mapped domain, i.e., it keeps the differential arc lengths as constant as possible at all points of the mapped surface. The goal of this work is to introduce the constant speed parametrization mapping of MoM-SIE surfaces and its approximation using large Lagrange quadrilateral patches, and to explain and emphasize the importance, in general, of achieving the constant speed parametrization (arc-length parametrization) along the surface coordinate lines, in an exact or approximate fashion, in order to obtain final analysis results with the best possible accuracy, considering the degrees of freedom used to describe the geometry. Note that an interesting example of a CEM application of the arc-length parametrization can be found

Manuscript received November 09, 2011; accepted December 08, 2011. Date of publication December 16, 2011; date of current version January 02, 2012. This work was supported by the National Science Foundation under Grants ECCS-0650719 and ECCS-1002385 and the Serbian Ministry of Science and Technological Development under Grant TR-32005.

M. M. Ilić is with the School of Electrical Engineering, University of Belgrade, 11120 Belgrade, Serbia, and also with the Department of Electrical and Computer Engineering, Colorado State University, Fort Collins, CO 80523-1373 USA (e-mail: milanilic@etf.rs).

S. V. Savić is with School of Electrical Engineering, University of Belgrade, 11120 Belgrade, Serbia (e-mail: ssavic@etf.rs).

A. Ž. Ilić is with the Laboratory of Physics 010, Vinča Institute of Nuclear Sciences, 11001 Belgrade, Serbia (e-mail: andjelijailic@ieee.org).

B. M. Notaroš is with the Department of Electrical and Computer Engineering, Colorado State University, Fort Collins, CO 80523-1373 USA (e-mail: notaros@colostate.edu).

Color versions of one or more of the figures in this letter are available online at http://ieeexplore.ieee.org.

Digital Object Identifier 10.1109/LAWP.2011.2180354

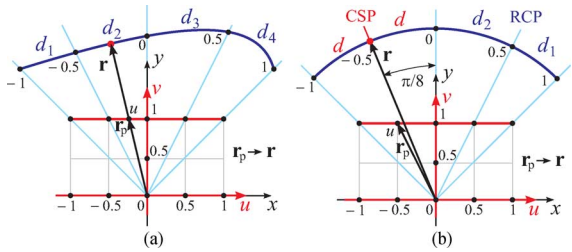

Fig. 1. Parent-line to parametric-curve mapping for (a) an arbitrary curve and (b) a quarter of a circular arc.

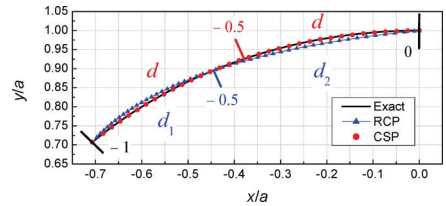

Fig. 2. Geometrical modeling of an eighth of a circular arc based on approximations of the RCP and CSP mappings, respectively, using second-order Lagrange parametric curves. Distances between interpolation nodes according to RCP and CSP mappings are also indicated.

in [10], where it is adopted in the context of directivity and impedance optimizations of planar curved wire antennas. This letter also derives simple formulas for the exact mapping of parent line segments and squares to circular arcs and spherical sections, respectively, which result in uniformly or almost uniformly spaced interpolation nodes in the projected domain, thus keeping the least amount of distortion, and which, in that respect, differ from conventional mapping formulas based on the central projection parametrization (ray casting). Furthermore, it demonstrates the general applicability of the constant speed parametrization (CSP) mapping to more complex curved surfaces by positioning the Lagrange interpolation nodes so that the equidistant points in the parent domain are also equidistant along the corresponding projected arcs in the child domain through a numerical solution to a set of resulting CSP equations in the parametric space.

II. Ray Casting and Constant Speed Parametrization Geometrical Mappings

Consider an arbitrary curve that needs to be parametrized for the purposes of CEM simulation, as shown in Fig. 1(a). To this end, we start from the parametric equation for the line segment in the parent domain, $\mathbf{r}_\mathrm{p} = u\mathbf{i}_x + \mathbf{i}_y$, $-1 \le u \le 1$, $v = 1$, and seek a transformation in the form $\mathbf{r}(u) = x(u)\mathbf{i}_x + y(u)\mathbf{i}_y$. Conventionally, the mapping of the line segment is done by projecting it onto the curve with the common center as the projection center (an analogous procedure for square-to-surface mapping is given in [11] and [12]). This type of mapping can be referred to as the ray-casting parametrization (RCP) mapping, given the analogy with ray-casting applications in computer graphics [13], [14]. Applied to a quarter of a circular arc of radius a, shown in Fig. 1(b), the RCP mapping is then easily derived as

$$\mathbf{r}(u) = a\frac{\mathbf{r}_\mathrm{p}(u)}{|\mathbf{r}_\mathrm{p}(u)|} = a\frac{u\mathbf{i}_x + \mathbf{i}_y}{\sqrt{1+u^2}} \tag{1}$$

and the rate of change of differential arc lengths on the curve comes out to be $\mathrm{d}l/\mathrm{d}u = \sqrt{(\partial x/\partial u)^2 + (\partial y/\partial u)^2} = a/(1+u^2)$, so that it can be clearly seen in the right-hand half of Fig. 1(b) that the RCP yields nonequidistant projections of parent interpolation nodes ($d_1 < d_2$). However, we introduce here a different mapping, as depicted in the left-hand half of Fig. 1(b), where the interpolation node at $u = -0.5$ is mapped to the middle of the left-hand half of the arc, which results in uniformly spaced nodes on the parametric curve. The associated $\mathbf{r}_\mathrm{p} \to \mathbf{r}$ transformation is given by

$$\mathbf{r}(u) = a\sin\left(\frac{\pi u}{4}\right)\mathbf{i}_x + a\cos\left(\frac{\pi u}{4}\right)\mathbf{i}_y \tag{2}$$

for which $\mathrm{d}l/\mathrm{d}u = a\pi/4$ is constant. We call this type of mapping the CSP mapping, as the speed with which the mapped point traces the curve, expressed in terms of the parameter (u), is constant along the curve (for $-1 \le u \le 1$).

To demonstrate the difference resulting from approximations of the mappings in (1) and (2) by Lagrange elements, we model the left-hand half of the circular arc in Fig. 1(b) by a second-order ($K_u = 2$) Lagrange curve using three equidistant interpolation nodes obtained by RCP and CSP mappings, respectively, and plot the results in Fig. 2. It can be seen that the CSP curve approximates the arc geometrically almost exactly, whereas the RCP curve deviates from it, albeit only slightly. Thus, it is to be expected that any models with the CSP mapping will yield better results. Furthermore, the computed $\mathrm{d}l/\mathrm{d}u$ is much more uniform for the CSP curve. Hence, in addition to a higher geometrical accuracy, we expect better solutions with the CSP mapping than with the RCP one because the surface-current densities in MoM modeling are expressed as functions of coordinates in the parent domain, i.e., u and v (on generalized quadrilaterals), in which integrations and testing are performed as well, and with respect to which the approximation of the CSP mapping introduces less distortion.

We next consider mapping from a square parent domain to one-sixth of a sphere (of radius a). The exact RCP mapping, found analogously to (1) [11], [12], is illustrated in the left inset of Fig. 3, where similar problems as in Fig. 1 with distortion of the projected parametric space are observed. The use of the CSP mapping, with keeping the points uniformly distributed along the corresponding parts of the two great circles on the spherical patch, again can overcome the problems. As a generalization of (2), the resulting exact CSP mapping is given by

$$h(u,v) = \sqrt{1 + \tan^2\left(\frac{\pi u}{4}\right) + \tan^2\left(\frac{\pi v}{4}\right)}$$
$$x = \frac{a\tan\left(\frac{\pi u}{4}\right)}{h} \quad y = \frac{a\tan\left(\frac{\pi v}{4}\right)}{h} \quad z = \frac{a}{h} \tag{3}$$

and this is depicted in the right inset of Fig. 3.

In general, explicit analytical expressions for the CSP mappings are difficult or impossible to find. Instead, positioning the Lagrange interpolation nodes such that the equidistant points in the parent domain are also equidistant along the corresponding

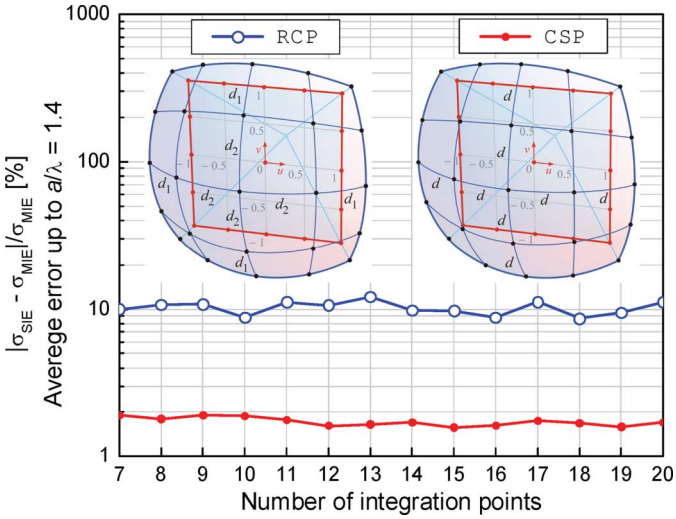

Fig. 3. MoM-SIE analysis of a dielectric ($\varepsilon_r = 4$) spherical scatterer (six quadrilaterals, $K_u = K_v = 4$, and $N_u = N_v = 6$), using RCP and CSP mapping models: absolute relative RCS error averaged over multiple values of a/λ versus the number of integration points in the Gauss–Legendre formula (with details of RCP and CSP square-to-surface mappings depicted in the insets).

projected arcs in the child domain is sufficient and can be carried out numerically along an arbitrary parametric line, as will be demonstrated in an example in Section III.

Finally, note that although the CSP mapping is presented in this letter in conjunction with Lagrange curvilinear parametric elements, it can as well be applied to any curve or surface defined by mathematical equations, including those using NURBS [15]. Namely, any curve can be reparametrized to achieve constant speed parametrization [16], which, in general, must be done numerically [15].

III. Numerical Results of 3-D MoM-SIE EM Modeling Using RCP and CSP Mappings

As the first example of 3-D MoM-SIE EM modeling using RCP and CSP mapping approaches, consider a dielectric ($\varepsilon_r = 4$, $\mu_r = 1$) spherical scatterer of radius a in free space. The spherical surface is modeled by means of six Lagrange quadrilateral patches of the fourth geometrical order ($K_u = K_v = 4$), and with polynomial divergence-conforming hierarchical basis functions [3] of order $N_u = N_v = 6$ in both directions (u and v) for electric and magnetic surface current density vectors on all patches. It is found that the CSP model, which gives accurate results for the monostatic radar cross section (RCS) up to the frequency at which $a/\lambda = 2$, λ being the wavelength in the dielectric, performs much better than the RCP model, which results in noticeable errors even starting from relatively low frequencies (where $a/\lambda \approx 0.42$) and definitely performs poorly at frequencies where $a/\lambda > 1.4$. In addition, Fig. 3 presents the respective percentage errors of the RCS calculation [with respect to the analytical solution (Mie's series)] averaged over the frequency range up to where $a/\lambda = 1.4$ versus the number of integration points (using the Gauss–Legendre integration formula) in each direction of quadrilateral patches in MoM-SIE solutions. We conclude from the figure that while both models produce numerically stable solutions, the CSP model gives five times lower average error in the considered frequency span.

As the second example, in order to independently identify the sole influence of the parametrization on the solution accuracy, we consider a metallic square plate scatterer (of side length $a = 1$ m), which is geometrically exactly represented by a flat quadrilateral. While the computed RCS at a frequency of $f = 550$ MHz for the CSP model (standard quadrilateral with $K_u = K_v = 1$) agrees very well with a completely hp-refined reference solution by WIPL-D, the result for a non-CSP quadrilateral with $K_u = K_v = 4$ for which we offset the control points at $v = \pm 0.5$ by ± 0.1 m differs by 46%. The accuracy gain in the current distribution over the plate is even more pronounced.

As the last example and a demonstration of the general applicability of the CSP mapping to more complex curved surfaces (arbitrarily defined by some sort of mathematical equations), we perform CSP modeling and scattering analysis of the metallic double ogive, a benchmark target established by the Electromagnetic Code Consortium (EMCC), at a frequency of $f = 1.57$ GHz [17]. First, the ogive is meshed (based on geometrical equations from [17]) using 24 MoM quadrilateral patches with $K_u = K_v = 4$, and the model appears in the inset of Fig. 4. Next, the CSP algorithm is applied to parameter ranges -2.5 in $< t < 0$ and $0 < t < 5$ in, respectively. For a parametric line defined by $x(t), y(t), z(t)$, we stipulate that the partial arc lengths between any two points are equal to one another, and equal to $1/N$ of the total arc length spanned by t, where N is the number of segments required within the parameter span. This is done by numerically solving the set of equations

$$\int_{t=t_0}^{t_{xOy,i}} \sqrt{\left(\frac{\partial x}{\partial t}\right)^2 + \left(\frac{\partial y}{\partial t}\right)^2 + \left(\frac{\partial z}{\partial t}\right)^2}\,\mathrm{d}t = \frac{i}{8}\int_{t=t_0}^{t_8} \sqrt{\left(\frac{\partial x}{\partial t}\right)^2 + \left(\frac{\partial y}{\partial t}\right)^2 + \left(\frac{\partial z}{\partial t}\right)^2}\,\mathrm{d}t, \quad i = 0, 1, \ldots, 7 \tag{4}$$

$$\int_{t=t_{xOy,i}}^{t_{24}} \sqrt{\left(\frac{\partial x}{\partial t}\right)^2 + \left(\frac{\partial y}{\partial t}\right)^2 + \left(\frac{\partial z}{\partial t}\right)^2}\,\mathrm{d}t = \frac{24-i}{16}\int_{t=t_8}^{t_{24}} \sqrt{\left(\frac{\partial x}{\partial t}\right)^2 + \left(\frac{\partial y}{\partial t}\right)^2 + \left(\frac{\partial z}{\partial t}\right)^2}\,\mathrm{d}t, \quad i = 9, 10, \ldots, 24 \tag{5}$$

where $t_0 = -2.4925$ in and $t_{24} = 4.9925$ in (the very tip points of the two half-ogives are excluded), and $t_{xOy,8} = 0$ (there is a jump discontinuity at the $t = 0$ plane), using a standard secant method for numerical root finding and evaluating all the integrals numerically as well. The solutions are parameters t arranged in the CSP manner in the xOy-plane ($t_{xOy,i}$, $i = 0, 1, \ldots, 24$). On the other hand, as the ogive is rotationally symmetric, the CSP distribution of the ψ parameter ($0 < \psi < 2\pi$) is given by $\psi_j = j2\pi/16$, $j = 0, 1, \ldots, 15$. Finally, interpolation nodes (that define MoM patches) are obtained by substituting parameters t_{xOy} and ψ into geometrical equations of the ogive in [17]. Higher-order MoM CSP results with $N_u = N_v = 3$ (total number of unknowns is 420) for the RCS of the double ogive are compared in Fig. 4 with simulation

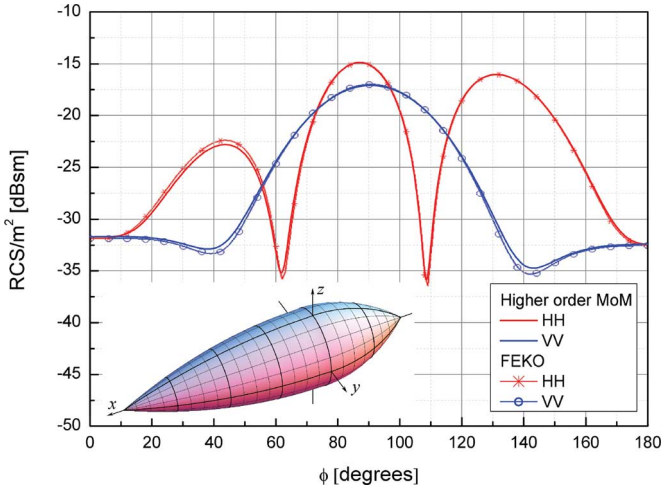

Fig. 4. RCS of the metallic double ogive at $f = 1.57$ GHz [17] as a function of the azimuthal angle (the elevation angle is zero) for the horizontal (HH) and vertical (VV) polarizations, respectively: comparison of the higher-order MoM-SIE solution using CSP parametrization with results obtained by FEKO [18]; geometrical model with 24 curved ($K_u = K_v = 4$) quadrilateral elements is shown in the figure inset.

results obtained by FEKO [18], and an excellent agreement of the two sets of results is observed.

IV. Conclusion

This letter has introduced a constant speed parametrization mapping of MoM-SIE boundary surfaces in analysis of antennas and scatterers and its approximation using large Lagrange-type quadrilateral patches and has demonstrated the importance of achieving, at least approximately, the constant speed parametrization (arc-length parametrization) along the surface coordinate lines. The proper placement of interpolation nodes that ensures minimum mapped parametric space distortion is especially important when large high-order curvilinear elements are constructed and applied. In 3-D MoM-SIE analysis of a spherical scatterer, the CSP cube-to-sphere mapping has resulted in on average five times lower percentage error in RCS computations than with the ray-casting parametrization mapping. The RCS results have confirmed all conclusions and expectations derived from the analysis of geometrical results in Fig. 2. Moreover, we realize that what appeared as slight geometrical inaccuracies in the model actually translates into rather considerable errors in the RCS, which emphasizes even more the importance of proper geometrical mapping, namely, CSP mapping in the higher-order MoM-SIE case. The proposed CSP mapping concept has been extended to arbitrary curves and surfaces (defined by some sort of parametric equations) employing a numerical solution to a set of resulting CSP equations in the parametric space, which has been demonstrated in 3-D MoM-SIE modeling of the EMCC double-ogive target.

References

[1] P. P. Silvester and R. L. Ferrari, *Finite Elements for Electrical Engineers*. Cambridge, U.K.: Cambridge Univ. Press, 1996.

[2] B. M. Notaroš, "Higher order frequency-domain computational electromagnetics," *IEEE Trans. Antennas Propag.*, vol. 56, no. 8, pp. 2251–2276, Aug. 2008.

[3] M. Djordjevic and B. M. Notaros, "Double higher order method of moments for surface integral equation modeling of metallic and dielectric antennas and scatterers," *IEEE Trans. Antennas Propag.*, vol. 52, no. 8, pp. 2118–2129, Aug. 2004.

[4] J. P. Swartz and D. B. Davidson, "Curvilinear vector finite elements using a set of hierarchical basis functions," *IEEE Trans. Antennas Propag.*, vol. 55, no. 2, pp. 440–446, Feb. 2007.

[5] G. Kang, J. Song, W. C. Chew, K. C. Donepudi, and J. M. Jin, "A novel grid-robust higher order vector basis function for the method of moments," *IEEE Trans. Antennas Propag.*, vol. 49, no. 6, pp. 908–915, Jun. 2001.

[6] W. Ding and G. Wang, "Treatment of singular integrals on generalized curvilinear parametric quadrilaterals in higher order method of moments," *IEEE Antennas Wireless Propag. Lett.*, vol. 8, pp. 1310–1313, 2009.

[7] M. S. Tong and W. C. Chew, "A higher-order Nyström scheme for electromagnetic scattering by arbitrarily shaped surfaces," *IEEE Antennas Wireless Propag. Lett.*, vol. 4, pp. 277–280, 2005.

[8] E. Martini, G. Pelosi, and S. Selleri, "A hybrid finite-element-modal-expansion method with a new type of curvilinear mapping for the analysis of microwave passive devices," *IEEE Trans. Microw. Theory Tech.*, vol. 51, no. 6, pp. 1712–1717, Jun. 2003.

[9] L. Valle, F. Rivas, and M. F. Cátedra, "Combining the moment method with geometrical modelling by NURBS surfaces and Bézier patches," *IEEE Trans. Antennas Propag.*, vol. 42, no. 3, pp. 373–381, Mar. 1994.

[10] J. Kataja and K. Nikoskinen, "The parametric optimization of wire dipole antennas," *IEEE Trans. Antennas Propag.*, vol. 59, no. 2, pp. 350–356, Feb. 2011.

[11] B. M. Kolundzija and B. D. Popovic, "Entire-domain Galerkin method for analysis of metallic antennas and scatterers," *Proc. Inst. Elect. Eng. H*, vol. 140, no. 1, pp. 1–10, Feb. 1993.

[12] B. M. Kolundzija and A. R. Djordjević, *Electromagnetic Modeling of Composite Metallic and Dielectric Structures*. Norwood, MA: Artech House, 2002.

[13] *An Introduction to Ray Tracing*, A. S. Glassner, Ed. San Francisco, CA: Morgan Kaufmann, 1989.

[14] A. De Cusatis Jr., L. H. De Figueiredo, and M. Gattass, "Interval methods for ray casting implicit surfaces with affine arithmetic," in *Proc. 12th Brazilian Symp. Comput. Graphics Image Process.*, 1999, pp. 65–71.

[15] G. Casciola and S. Morigi, "Reparametrization of NURBS curves," *Int. J. Shape Model.*, vol. 2, no. 2 & 3, pp. 103–116, 1996.

[16] B. O'Neill, *Elementary Differential Geometry*, 2nd ed. Amsterdam, The Netherlands: Elsevier, 2006.

[17] A. C. Woo, H. T. G. Wang, M. J. Schuh, and M. L. Sanders, "Benchmark radar targets for the validation of computational electromagnetics programs," *IEEE Antennas Propag. Mag.*, vol. 35, no. 1, pp. 84–89, Feb. 1993.

[18] "FEKO," EM Software & Systems-S.A. (Pty) Ltd., Stellenbosch, South Africa, 2011 [Online]. Available: http://feko.info/applications/RCS